IEEE Access
Multidisciplinary | Rapid Review | Open Access Journal

Received January 29, 2021, accepted March 4, 2021, date of publication March 9, 2021, date of current version March 17, 2021.

Digital Object Identifier 10.1109/ACCESS.2021.3064950

Power Profile-Based Antenna Selection for Millimeter Wave MIMO With an All-Planar Lens Antenna Array

QIANYUN ZHANG[1], (Member, IEEE), XINWEI LI[1], (Student Member, IEEE), LEI CHENG[2], YUANWEI LIU[3], (Senior Member, IEEE), AND YUE GAO[4], (Senior Member, IEEE)

[1]School of Cyber Science and Technology, Beihang University, Beijing 100191, China
[2]Shenzhen Research Institute of Big Data, Shenzhen 518000, China
[3]School of Electronic Engineering and Computer Science, Queen Mary University of London, London E1 4NS, U.K.
[4]Department of Electrical and Electronic Engineering, University of Surrey, Surrey GU2 7XH, U.K.

Corresponding author: Lei Cheng (leicheng@sribd.cn)

This work was supported in part by the National Natural Science Foundation of China (NSFC) under Grant 61901020, in part by the Open Research Fund from Shenzhen Research Institute of Big Data under Grant 2019ORF01012, and in part by the Liaoning Collaboration Innovation Center for CSLE.

ABSTRACT Lens antenna arrays can significantly reduce the number of radio frequency (RF) chains and provide a cost-effective beamforming approach to millimeter-wave massive multiple-input multiple-output (MIMO) systems. However, the presence of curved fronts has imposed practical challenges in fabrication and system integration as the antennas have to be deployed on the lens focal curve or face. To this end, we analyze the massive MIMO system with an all-planar RF lens antenna array whose lens is made of metamaterials and the antennas are distributed on a two-dimensional (2D) plane. In terms of this structure, we then propose a power-profile based antenna selection method. Specifically, by considering the coupling among antenna elements and that between the RF-lens and the antenna array, the analyses regard the lens and antennas as an entity using a full-wave model. Antennas are selected according to the angle of arrivals (AoAs) of signals transmitted by users and the lens response to the incident wave from an arbitrary direction on antennas. Simulations are provided for verifying the system performance and to show: i) Specific gain responses on each element of the base station antenna array for user terminals distributed at different locations; and ii) The all-planar lens antenna array supports a spectrum efficiency upto 170.7 bps/Hz for a 25 GHz MIMO system with 50 user terminals and a signal-to-noise ratio (SNR) of 10 dB.

INDEX TERMS Antenna array, antenna selection, millimeter wave communication, MIMO, RF-lens.

I. INTRODUCTION

The fifth generation (5G) mobile communication system has developed rapidly over the past few years, and today dozens of countries have launched commercial 5G services [1]. Compared with previous systems, the application of 5G calls for a massive access, ultra-low latency and large capacity service. Out of these considerations, the 5G mobile communication system introduces technologies like millimeter-wave communication, large-scale antenna deployment, heterogeneous network fusion, and *et al.* to comprehensively upgrade the network performance [2]–[5].

The associate editor coordinating the review of this manuscript and approving it for publication was Yasar Amin.

Benefiting from abundant continuously available spectrum resources, the millimeter-wave (mmWave) frequency band is easy to meet the requirements of the ultra-high communication rate and bandwidth of 5G communication systems. However, mmWave signals generally suffer from more significant path loss than lower frequency bands. To maintain sufficient link gains, a large number of antennas are typically required at the base station for highly directional communications, and corresponding beamforming techniques have been widely explored and applied in mmWave systems [6]–[13]. Combining analog beamforming with digital precoding, the hybrid beamforming technology has become the contemporary mainstream method [10]–[13]. In this scheme, signals captured by the antenna array are processed to radio frequency (RF) chains through an analog

processing network composed of RF components like phase shifters and amplifiers. As each antenna usually requires one dedicated RF chain, mmWave massive multiple-input multiple-output (MIMO) is in practice difficult to deploy due to unaffordable hardware cost and energy consumption from RF components [14], [15]. To mitigate these issues, the beamspace MIMO has been recently proposed to significantly reduce the number of RF chains by employing a lens antenna array, which integrates a lens with an antenna array as the feeding structure [16]. Converting a divergent wavefront from an antenna element into a plane wave and vice versa, the lens antenna array transforms the conventional spatial channel to the beamspace channel. As each beam corresponds to one RF chain in beamspace MIMO, this structure captures the channel sparsity at mmWave frequencies and significantly reduce the required RF chains [17]. Researches have demonstrated the advantages of high gain and a narrow beamwidth of this structure and its superior performance on energy efficiency [16]–[18]. Based on the lens antenna systems, subsequent work has explored the beam selection schemes [19], [20], beamspace channel estimation techniques [21], [22], link budget estimation [23], and etc. Their performance on MIMO non-orthogonal multiple access (NOMA) systems [24], [25], wireless local area network (WLAN), and wireless personal area network (WPAN) communication systems [26], [27] has also been evaluated.

To evaluate the system performance of the RF-lens equipped antenna array, the energy focusing profile for different angle of arrivals (AoAs) on different antenna elements caused by the lens is the key. Therefore, various methods have been used to model the lens response. In [16], [17], [24], [28], by ignoring the side lobes, the lens was approximately modelled as a spatial discrete Fourier transform (DFT) matrix, and each beamspace signal was mapped onto a corresponding orthogonal beam. To further improve the model accuracy of the lens antenna, in [26], the energy focusing or beam collimation was derived analytically based on the electromagnetic ray propagation phase delay and constructive superposition principles, and the work demonstrated that the array response follows a "sin" function in terms of the AoA and the antenna locations. Afterwards, the work was extended to a full-dimensional lens antenna array where the feeding antenna elements locate at the focal surface of the lens [27]. The aforementioned work derived the lens model by treating its thickness negligible, while in practice, the thickness of a lens can be comparable to the antenna operating frequency [29]. Taking an electromagnetic lens model into consideration, the electric field distributions of the lens model under different incident waves were simulated in an electromagnetic simulation tool, and the main beam and two adjacent side lobes were considered in the system analyses [18]. In [30], the beam propagation method (BPM) was used to estimate the power profile of a dielectric RF lens. Although quite efficient in terms of calculation, the BPM is based on the Fourier optics and applies only to an electrically large homogenous dielectric lens. Moreover, prior studies have not taken the coupling between the lens and antennas into consideration. For the complete and rigorous study of the RF-lens equipped antenna array, the antenna elements and lens components should be studied simultaneously in a unified model.

In addition, common lenses are built using dielectric material with curved front or rear surfaces [31], [32], which always make them bulky and difficult to be integrated into modern compact systems. Recent years, planar lens made of inhomogeneous materials or metamaterials [33]–[35] have been developed to improve the integration density or compactness of the communication system. Last but not the least, the lens response arrays were derived with the feeding antenna array located at the focal curve or the focal face, while this curved deployment is difficult for practical fabrication and system integration. Planar feed antenna structures such as microstrip patch antenna array for microwave band and substrate integrated waveguide (SIW) slot array for millimeter-wave band are easy to fabricate and to integrate with other planar circuits in a coplanar way.

In this paper, we first design an all-planar lens antenna array for practical antenna integration and deployment. Specifically, metamaterials are employed to construct a planar RF-lens, and its feeding antenna array is arranged in a two-dimensional (2D) plane. To obtain an accurate channel model for mmWave massive MIMO systems with the designed lens antenna array, we first employ a full-wave numerical model to obtain the power received by each antenna for the incident wave with an arbitrary direction. In this way, the mutual electromagnetic coupling among antenna elements and between the antenna array and RF lens are considered. Besides, incident waves with both vertical and horizontal polarizations are analyzed and combined for a complete study. Next, to evaluate the system performance of the all-planar lens antenna array, we consider a typical mmWave massive MIMO system, where the base station employs the metamaterial-based all-planar lens antenna array to simultaneously serve multiple single-antenna users. The channel matrix is determined according to the aforementioned analysis model, and a corresponding antenna selection procedure based on the array power profile is subsequently proposed and applied. Interference among antennas is eliminated at the digital processing stage. Simulation results are finally provided to validate the effectiveness of the proposed lens antenna array analysis and operation schemes.

The rest of this paper is organized as follows. Section II presents the system architecture, and with the extra gain introduced by the RF lens, the channel model is clarified as well. Next, power profiles of all antenna elements with various directions of incident waves are calculated by combining the lens and 2D antenna array in an entity in Section III. In Section IV, a novel antenna selection scheme is proposed based on the power profile obtained before, and the system performance of the all-planar RF lens antenna array is simulated and discussed with different user distributions and noise levels. Finally, the conclusion is drawn in Section V.

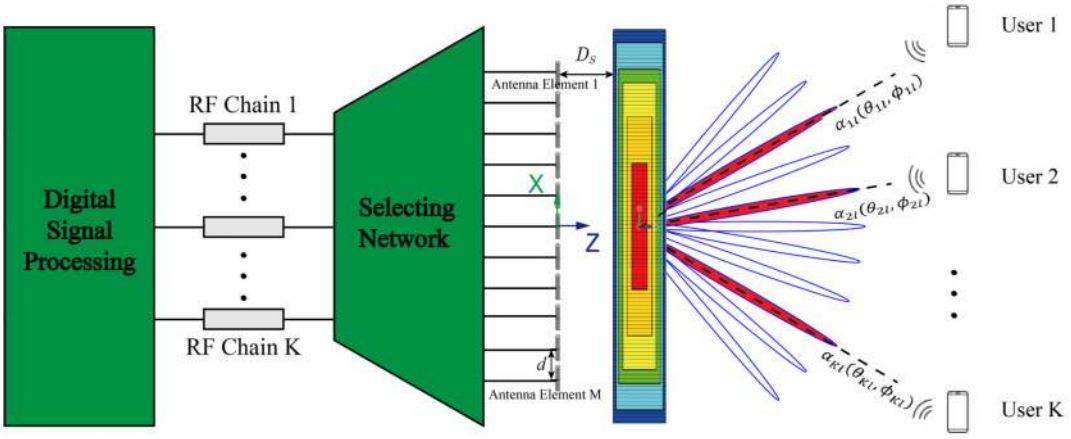

FIGURE 1. System architecture of a mmWave massive MIMO with the proposed metamaterial-based planar lens antenna array.

Notation: Bold uppercase letters denote matrices and bold lowercase letters denote vectors. a_{ij} is the $(i,j)^{\text{th}}$ entry of $\mathbf{A}$ and i^{th} entry of $\mathbf{a}_j$. $||\mathbf{A}||$ denotes the Frobeius norm, $\mathbf{A}^{-1}$ is the inverse, $\mathbf{A}^T$ is the transpose, and $\mathbf{A}^H$ is the Hermitian transpose of $\mathbf{A}$, respectively. $\mathbf{I}_N$ is the unitary matrix with dimension N.

II. SYSTEM MODEL

We consider the uplink scenario of a mmWave massive MIMO communication system. As shown in Fig. 1, K mobile user terminals equipped with single antenna send independent messages to the base station. The planar lens antenna array equipped at the base station composes of a M-element antenna array and a metamaterial-composed RF-lens, and its perspective view is illustrated in Fig. 2. User terminals transmit their signals at distinct beamspace channels to avoid the intra-beam interference, and the baseband equalization is applied at the digital processing stage to control the interference among users. Thus, the signal received by the base station can be expressed as

$$y = \mathbf{FHs} + \mathbf{n}, \tag{1}$$

where $\mathbf{s} = [p_{t1}s_1, p_{t2}s_2, \ldots, p_{tK}s_K]^T$ is the $K \times 1$ transmitted signals vector. p_{tk} is the transmission power for each user, and $\mathbb{E}[ss^*] = I_K$. $H = [h_1, h_2, \ldots, h_K]$ is the $M \times K$ channel matrix containing the path loss and the power gain at the base station. F denotes the equalization filter at the base station with a dimension of $K \times M$. n_k is the Gaussian noise presented at the kth antenna, i.e. $n \sim \mathcal{N}(0, \sigma_j^2 I)$.

Under the far-field condition, we can assume the transmitted signal from the kth user arrives at the base station antenna array via L_k paths, $l = 1, 2, \ldots, L_k$ by the AoA $\alpha_{kl}(\theta_{kl}, \phi_{kl})$. The channel coefficients h_{mk} between the kth user and the mth antenna element of the base station equipped with a RF lens can be written as [18]:

$$h_{mk} = \frac{\sqrt{\beta_k}}{\sqrt{L_k}} \sum_{l=1}^{L_k} \sqrt{g_{kl}} a_{kl}^m \exp\left(j\psi_{kl} + j\frac{2\pi}{\lambda}\Delta_m^{kl}\right), \tag{2}$$

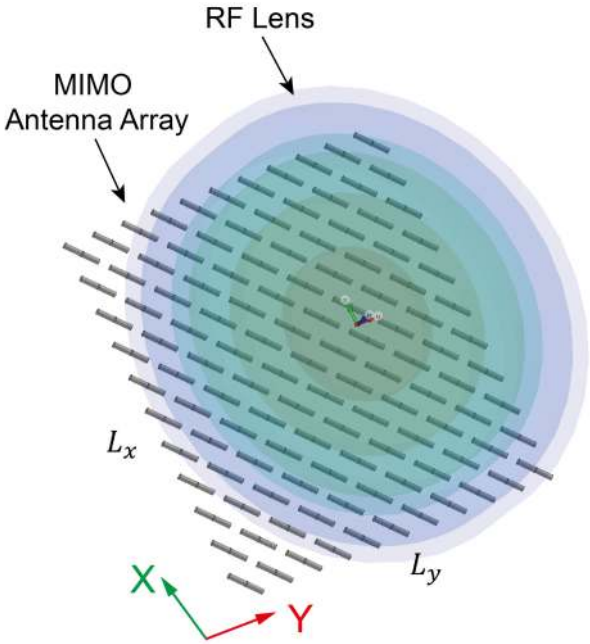

FIGURE 2. Perspective view of the metamaterial-based planar lens antenna array.

where $j = \sqrt{-1}$ is the imaginary unit and β_k is the large-scale fading coefficient including the effects of path-loss and shadowing. g_{kl} is the power gain of the lth path for user k such that $(1/L_k)\sum_{l=1}^{L_k} \mathbb{E}[g_{kl}] = 1, \forall k$; ψ_{kl} denotes the phase shift introduced by the lth path, and ψ_{kl} for $l = 1, 2, \ldots, L_k$ are independently and identically distributed (i.i.d) random variables with uniform distribution over $[0, 2\pi]$. a_{kl}^m represents the effect of AoA-dependent energy gain and phase delay introduced by the RF lens. It corresponds to the focused energy captured by the mth antenna element for the incident plane wave from the kth user through the lth path, and if the lens is absent, i.e. all a_{kl}^m equal to 1, $\mathbb{E}\left[|h_{mk}|^2\right] = \beta_k, \forall m$.

The antenna array of the proposed lens antenna array is assumed to be a 2D planar array with $M = L_x L_y$ elements

in total. Distance between the antenna plane and the RF lens is D_s, and it is determined by the focal length of the lens. For electromagnetic isolation and compactness, antennas have a equal distance of $d \sim \lambda/2$ and λ is the free-space wavelength at the center frequency. As shown in Fig. 2, the planar array locates on the $z = 0$ plane, and the normal unit vector pointing to the lens is z-axis direction. Thence,position of the mth antenna (x_m, y_m) is then given by

$$\begin{aligned} x_m &= -(L_x - 1)d/2 + \lfloor (m-1)/L_y d, \\ y_m &= -(L_y - 1)d/2 + \mod(m-1, L_y)d \\ m &= L_x(j-1) + p, j = 1, 2, \ldots L_y; p = 1, 2, \ldots, L_x. \end{aligned} \tag{3}$$

The propagation distance difference of the mth element compared to the element at (0, 0) is Δ_m^{kl} and is given by

$$\Delta_m^{kl} = x_m \cos\theta_{kl} \cos\phi_{kl} + y_m \sin\theta_{kl} \cos\phi_{kl}. \tag{4}$$

Similar to the case of one-dimensional linear array [18], the angle parameters θ_{kl} and ϕ_{kl} are characterized by the AoA of line of sight (LoS) angle θ_k, ϕ_k with two random offset $\vartheta_{kl}, \varphi_{kl}$ if we take multipath effect into consideration, which are independently distributed according to a center power azimuth spectrum (PAS) with zero means and angular spread (standard deviation) σ_ϑ and σ_φ [36]. In the extreme case where both σ_ϑ and σ_φ equals to zero, it corresponds to the line of sight environment. Two commonly used empirical model for the observed PAS are the Laplacian [36] and the Gaussian [37] distributions. With small angular spreads σ_ϑ and σ_φ for each user k, we apply the approximation as follow:

$$a_{kl}^m \approx a_k^m. \tag{5}$$

As a result, the channel model (2) can be simplified as:

$$h_{mk} = \frac{\sqrt{\beta_k}}{\sqrt{L_k}} a_k^m \sum_{l=1}^{L_k} \sqrt{g_{kl}} \exp\left(j\psi_{kl} + j\frac{2\pi}{\lambda}\Delta_m^{kl}\right), \tag{6}$$

where a_k^mrepresents the complex addition gain captured by the mth antenna element for incident wave at direction (θ_k, ϕ_k).

Define vector $\mathbf{h}_k = [h_{1k}, h_{2k}, \ldots, h_{Mk}]^T$ as the channel vector of mth attenna, the the covariance matrix is $\mathbf{R}_k = \mathbb{E}\left[\mathbf{h}_k \mathbf{h}_k^H\right]$. $\mathbf{R}_m$ is a positive semidefinite matrix with diagonal entries equal to $\beta_k |a_k|^2$. The channel matrix of the RF-lens massive MIMO system vares for different AoAs of the user. Therefore, an accurate estimation of these lens-introduced power is critical for base station to achieve optimal communication capacity and quality.

III. RF LENS RESPONSE

As mentioned above, the existing models for the RF lens response estimation are either oversimplified or with limited applicability. In this work, we consider obtaining the energy focusing profile of the RF lens in a unified model, i.e. the full-wave model derived from the Maxwell equation. With the fast development of the computational electromagnetics t and computation hardware, the system performance evaluation involving large-scale antenna array can now be efficiently realized by using hybrid-methods [38] or full-wave methods enhanced by fast solvers and parallel computing [39].

From the Friis transmission equation, the power received by the base station antenna is determined by the power P_t delivered by the user antenna and the effective area of the base station antenna A_r^m in the AoA, i.e.

$$P_r^m = A_r^m(\theta_k, \phi_k) P_t = G_r^m(\theta_k, \phi_k) \frac{\lambda^2}{4\pi} P_t, \tag{7}$$

where θ_k and ϕ_k is the AoA of the kth user and G_r^m is the receive antenna gain of $m-$th antenna. Due to the presence of RF lens in front of the antenna array, the gain pattern for each antenna is different. In the previous studies, these gain patterns are evaluated by using two steps. First, evaluate the gain pattern for the same antenna array without the lens and the energy focusing property of the lens, individually. The total gain is then obtained by multiplying these two factors.

In this work, we consider the antenna array and lens an entity. Referring to Fig. 2, all antennas at the base station are in the receiving mode and the antenna port is loaded with an impedance Z_L when it is connected with the RF front through a matching circuit. Assuming the impedance Z_L equals to the antenna input impedance, which results in no matching loss and the received power for the mth antenna is

$$P_r^m = \frac{1}{2}\mathfrak{Re}(V \cdot I^*), \tag{8}$$

where V is the voltage drop between two port ends and I the current passing through the port, and they are related by $V = Z_L I$. By varying the incident angle for different users and carrying out the simulation as shown in Fig. 2, the receiving power $P_r^m(\theta_k, \phi_k)$ of all antennas $m = 1, 2, \ldots, M$ can be determined by (8) simultaneously.

Assuming the metallic antenna is a perfectly electrical conductor, wherefore only electric currents exist on its surface. The electric field integral equation derived from the Maxwell equation is

$$\mathbf{E}_m^{\text{imp}} + Z_0 \mathcal{L}(\mathbf{J}_m) = 0, \quad \mathbf{r} \in \mathbf{S}_m, \tag{9}$$

where $\mathbf{J}_m$ is the electric current density of the mth antenna surface S_m and Z_0 is the free-space wave impedance. The imposed electric field $\mathbf{E}_m^{\text{imp}}$ on this mth antenna body contains three components: the electric field radiated by the rest antenna elements, the electric field radiated by the lens, and the incident field from the user on this antenna body.

$$\mathbf{E}_m^{\text{imp}} = \sum_{i=1, i\neq m}^{M} Z_0 \mathcal{L}(\mathbf{J}_i) + \mathbf{E}^{\text{lens}} + \mathbf{E}_m^{\text{inc}}. \tag{10}$$

In (9) and (10), the integrodifferential operator $\mathcal{L}$ derived from the Maxwell equations is

$$\mathcal{L}(\mathbf{X}) = -jk_0 \int_S \left[\mathbf{X} + \frac{1}{k_0^2}\nabla(\nabla' \cdot \mathbf{X})\right] G(\mathbf{r}, \mathbf{r}') d\tau'. \tag{11}$$

$G(\mathbf{r}, \mathbf{r}')$ is the free-space Green's function and k_0 is the free-space wavenumber. Using the equivalence principle, the radiation field from the inhomogeneous or metamaterial lens can be represented by the equivalent surface electric and magnetic current density $\mathbf{J}_L$ and $\mathbf{M}_L$,

$$\mathbf{E}^{\text{lens}} = Z_0\mathcal{L}(\mathbf{J}_L) + \mathcal{K}(\mathbf{M}_L), \tag{12}$$

$$\mathbf{H}^{\text{lens}} = \frac{1}{Z_0}\mathcal{L}(\mathbf{M}_L) + \mathcal{K}(\mathbf{J}_L), \tag{13}$$

where the integrodifferential operator $\mathcal{K}$ is defined as

$$\mathbf{K}(\mathbf{X}) = -\int_S \mathbf{X} \times \nabla G(\mathbf{r}, \mathbf{r}')d\tau'. \tag{14}$$

On the lens surface, the surface current density $\mathbf{J}_L$ and $\mathbf{M}_L$ are related to the electric field $\mathbf{E}_s$ and magnetic field $\mathbf{H}_s$ on the boundary by the condition

$$\mathbf{J}_L = \hat{n} \times \mathbf{H}_s = \hat{n} \times \left(\sum_{m=1}^{M} \mathcal{K}(\mathbf{J}_m) + \mathbf{H}^{\text{inc}}_{\text{lens}} + \mathbf{H}^{\text{lens}}\right), \tag{15a}$$

$$\mathbf{M}_L = \mathbf{E}_s \times \hat{n} = \left(\sum_{m=1}^{M} Z_0\mathcal{L}(\mathbf{J}_m) + \mathbf{E}^{\text{inc}}_{\text{lens}} + \mathbf{E}^{\text{lens}}\right) \times \hat{n}, \tag{15b}$$

in which $\hat{n}$ is the surface norm of the RF lens. Apparently, the field on the lens surface is the sum of fields radiated by all antennas and that from the kth user. Using the equivalent principle as mentioned above, the internal electric $\mathbf{E}$ inside the RF lens is equivalent to the following variational formulation

$$F(\mathbf{E}) = \frac{1}{2}\int_V \left[\frac{1}{\mu_r}(\nabla \times \mathbf{E}) \cdot (\nabla \times \mathbf{E}) - k_0^2\epsilon_r \mathbf{E} \cdot \mathbf{E}\right] dV + jk_0Z_0 \int_S (\mathbf{E}_s \times \mathbf{H}_s) \cdot \hat{n} dS, \tag{16}$$

where V is the volume of the RF lens and ϵ_r and μ_r is the relative permittivity and permeability of the lens, respectively. Due to the complex geometry or material constitutions of a RF lens, the minimum value of (16) can be solved by using the finite element method. As the electric and magnetic fields on the lens surface are already given in (15), combining (15) and (16), and taking the variational principle, the equation for the internal field inside the RF lens is

$$\begin{bmatrix} K_{II} & K_{IS} & 0 \\ K_{SI} & K_{SS} & B \\ 0 & P & Q \end{bmatrix} \begin{Bmatrix} E_I \\ E_S \\ H_S \end{Bmatrix} = \begin{Bmatrix} 0 \\ 0 \\ b \end{Bmatrix}, \tag{17}$$

where E_I represents unknowns for the internal electric field, and E_s and H_s are the unknowns for the electric and magnetic field on the lens surface. The block matrices K_{II}, K_{IS}, K_{SI}, K_{SS} and B are the sparse matrices produced by using the finite element method (FEM). Matrices P and Q are obtained by discretizing the integrodifferential operators in (15a) and (15b) using the method of moment (MoM), respectively. The right-hand side vector b is related to the field imposed on the RF lens, which includes the field radiated by all antenna bodies and the incident field from the user.

Organize all the unknown surface currents, the final equation system is

$$\begin{bmatrix} \mathcal{L}_{11} & \mathcal{L}_{12} & \cdots & \mathcal{L}_{1M} \\ \mathcal{L}_{21} & \mathcal{L}_{22} & & \mathcal{L}_{2M} \\ \vdots & & \ddots & \vdots \\ \mathcal{L}_{M1} & \mathcal{L}_{M2} & \cdots & \mathcal{L}_{MM} \\ \mathcal{L}_{L1} & \mathcal{L}_{L2} & \cdots & \mathcal{L}_{LM} \\ \mathcal{K}_{L1} & \mathcal{K}_{L2} & \cdots & \mathcal{K}_{LM} \end{bmatrix} \begin{Bmatrix} J_1 \\ J_2 \\ \vdots \\ J_M \\ J_L \\ M_L \end{Bmatrix} = \begin{Bmatrix} -E_1^{inc} \\ -E_2^{inc} \\ \vdots \\ -E_M^{inc} \\ -E_{lens}^{inc} \\ -H_{lens}^{inc} \end{Bmatrix}. \tag{18}$$

Dividing the antenna and lens surface into triangular meshes and discretizing the unknown currents with basis functions, the above equation can be discretized using MoM. Then, the current passing through all antenna ports and the corresponding voltage drop can be extracted from the current distribution on the antenna surface, and the received power for each antenna element can be calculated by using (8).

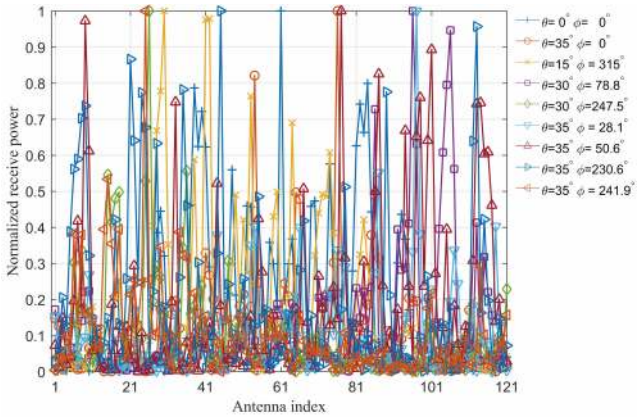

(a)

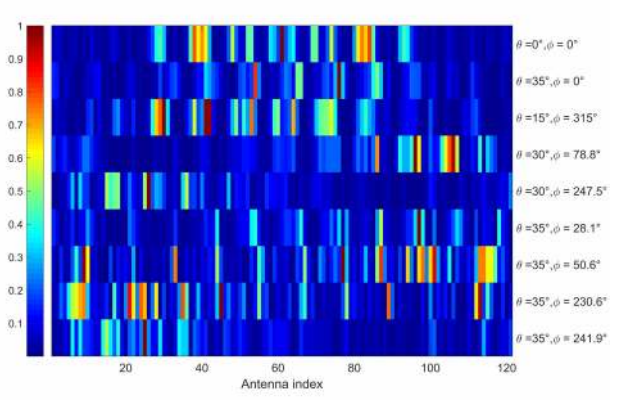

(b)

FIGURE 3. Normalized received power distribution on the proposed lens antenna array for vertically polarized plane waves with different AoAs: (a) received power curves; (b) power image where the intensity is represented by colored pixels.

The simulated power profiles for the total 121 antennas with different incident angles and polarizations are shown in Fig. 3 and Fig. 4. From these results, it is obvious that antenna elements have different gains to the incident plane wave with a particular AoA. Moreover, the received power

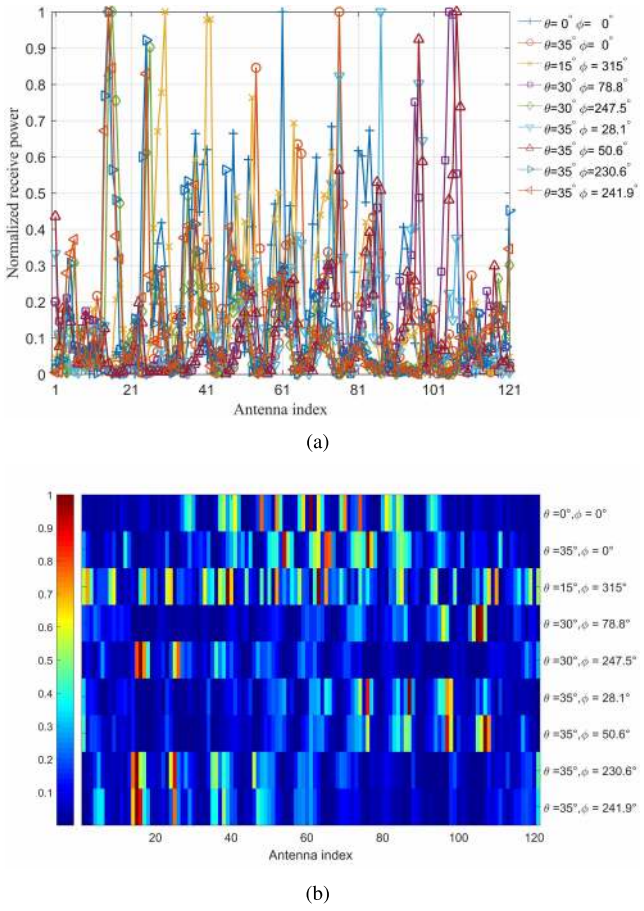

FIGURE 4. Normalized received power distribution on the proposed lens antenna array for horizontally polarized plane waves with different AoAs: (a) received power curves; (b) power image where the intensity is represented by colored pixels.

profile of the antenna elements varies for different polarizations, and thus the polarization should be taken into consideration when modelling a metamaterial-based lens antenna array. Last but not the least, for any incident angle, despite the polarization, peak of the received power appears at one antenna element, while unlike the DFT model, powers distributed at the rest antennas are not ignorable. As the DFT model is no longer valid for the proposed planar lens antenna array, the matching strategy between its antenna elements and users requires a reconsideration for efficient mmWave MIMO systems.

IV. ANTENNA SELECTION AND SYSTEM EVALUATION

A. POWER PROFILE-BASED ANTENNA SELECTION

In this section, with power distributions obtained from the proposed analysis model, an antenna selection scheme is developed to evaluate the achievable system performance of the designed metamaterial-based planar lens antenna array. To better demonstrate the power distribution, normalized total power profiles on the 11×11 antenna array for the vertical incident wave, and two oblique waves are given in Fig. 5. In this figure, the 2D planar antenna location information is also demonstrated for completeness. To optimize the system efficiency, selected antennas should produce the highest overall capacity to a corresponding set of users. In this subsection, a one-to-one matching scheme between users and antenna elements is established based on the signal AoAs and the power profile of the lens antenna array.

According to the system model given in (1), the signal-to-interference-plus-noise-ratio (SINR) of the kth user is

$$\gamma_k = \frac{\mathbf{f}_k \mathbf{h}_k}{\sum_{i=1, i\neq k}^{K} \mathbf{f}_k \mathbf{h}_i + \mathbf{f}_k \mathbf{f}_k^H \sigma^2}, \tag{19}$$

in which $\mathbf{f}_k$ is the kth row of the equalization filter matrix $\mathbf{F}$.

As the signal transmitted by one user generates responses on multiple antenna elements after passing through the RF-lens, the inter-beam interferences among users cannot be ignored. In this work, we adopt the zero-forcing (ZF) equalizer to suppress these interferences. Thus, the digital processing module in Fig. 1 can be represented in matrix as

$$\mathbf{F} = (\mathbf{H^H H})^{-1} \mathbf{H^H}. \tag{20}$$

Substituting (20) into (19), the SINR of kth user can be simplified to

$$\gamma_k = \frac{1}{\mathbf{f}_k \mathbf{f}_k^H \sigma^2}. \tag{21}$$

The achievable rate at the kth user is

$$R_k = \log_2 (1 + \gamma_k). \tag{22}$$

As a result, we have the capacity of all K users in the MIMO system as

$$R_{\text{sum}} = \sum_{k=1}^{K} R_k. \tag{23}$$

From (21)-(23), the total capacity of the MIMO system can be calculated from diagonal elements of matrix $\mathbf{F}\mathbf{F}^H$. This conclusion indicates that for a given group of users and channel conditions, instead of being affected by the one-to-one correspondence between users and antenna elements, the total channel capacity only relates to the set of selected antennas.

In order to maximize the spectrum efficiency, the exhaustive algorithm is a possible method. It computes channel capacities for all possible combinations of antenna subsets, and choose the subset that leads to the highest efficiency. However, for massive MIMO systems, such an approach can be computationally prohibitive because of the $\binom{M}{K}$ possible combinations. Therefore, inspired from the work presented in [40], we propose a decremental maximum capacity (DMC) antenna selection approach to the metamaterial-based all-planar lens antenna array mmWave MIMO system. According to the power profile obtained from the full-wave simulation analyses with polarization considered, the antenna selection scheme selects K antennas out of M by deleting those contributing the least to the system capacity one by one. As summarized in Algorithm 1, the presented procedure consists of $(M - K)$ loops. In the

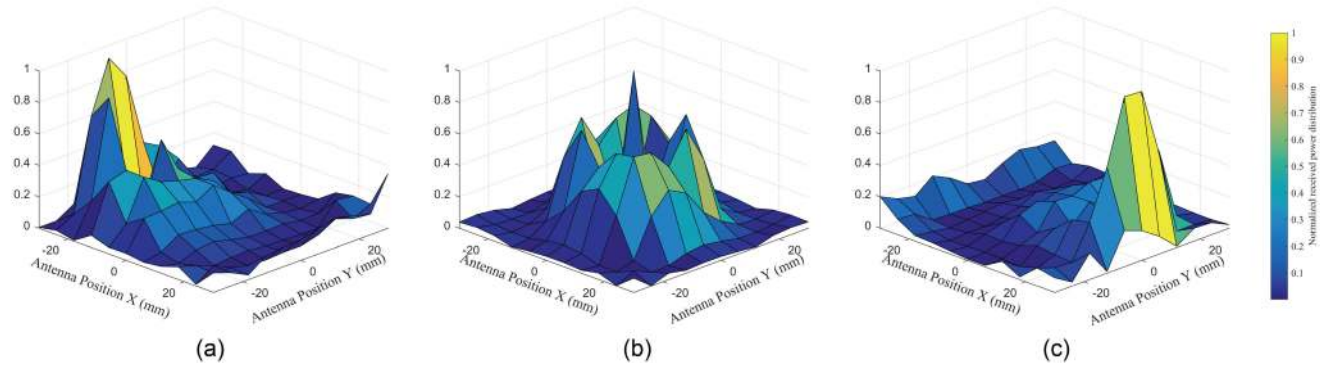

FIGURE 5. Normalized received power distribution of all antenna elements in the case of normal incidence (a) $\theta = 35°, \phi = 241.9°$, (b) $\theta = 0°, \phi = 0°$, and (c) $\theta = 30°, \phi = 78.8°$.

Algorithm 1 Power Profile-Based Decremental Maximum Capacity Antenna Selection

Input: $\mathbf{H}$
Output: $\tilde{\mathbf{H}}$
$\mathbf{A} = \mathbf{H}^T$
for $j = 1 \rightarrow M - K$ **do**
  for $k = 1 \rightarrow M - j + 1$ **do**
    $\mathbf{C}_k = (\mathbf{A}^{(k)H}\mathbf{A}^{(k)})^{-1}$
    $\mathbf{D}_k = diag\{\mathbf{C}_k\}$
    $R_k = \sum_{i=1}^{K} log_2(1 + \frac{1}{\sigma^2 \mathbf{D}_k(i)})$
  end for
  $\delta_j = \underset{j}{argmax}\{R_k\}$
  $\mathcal{D} = \{\delta_1, \delta_2, \cdots, \delta_j\}$
end for
$\tilde{\mathbf{A}} = [\mathbf{A}_{m,:}]_{m \notin \mathcal{D}}$
$\tilde{\mathbf{H}} = \tilde{\mathbf{A}}$

ith loop, channel capacities corresponding to the $(M - i + 1)$ antenna deletion strategies are calculated, and the antenna whose elimination causes the minimum capacity reduction is removed. Thus, $(M - K)(M - K + 1)/2$ calculations are required in this algorithm to achieve a near-optimal antenna selection. In this algorithm, $\mathcal{D}$ is the antenna subset removed in the antenna selection algorithm.

B. SIMULATION RESULTS

In this subsection, we provide simulation results to verify the system performance of the proposed all-planar lens antenna array-equipped massive MIMO system. The RF-lens antenna array composed of a flat metamaterial lens and an antenna array with 11 × 11 elements. The antenna power profile is obtained at a operation frequency of 25 GHz. To evaluate the system performance of the proposed all-planar RF lens antenna array, the gain of the lens is calculated from the ratio between received powers of antennas with a lens ($P_{withlens}$) and those of antennas without the lens (P_{nolens}) as follow

$$G = \frac{P_{withlens}}{P_{nolens}}, \tag{24}$$

TABLE 1. Average channel capacity (in bps/Hz) for different user numbers and channel SNRs.

SNR \ Users	10	20	30	40	50	60
-10 dB	0.067	0.044	0.031	0.026	0.017	0.012
0 dB	2.487	1.964	1.395	1.291	1.062	0.838
10 dB	5.495	4.540	3.872	3.448	3.021	3.012
20 dB	8.775	7.754	6.82	6.008	6.01	5.440
30 dB	12.065	11.06	10.74	9.567	8.492	8.11

where $P_{withlens}$ and P_{nolens} are obtained by applying horizontally and vertically polarized plane waves to the antenna system. Fig. 6 presents gains of the lens to incident waves from several representative AoAs.

In the simulation, users distribute over the angular spread of the antenna array with $0° \leq \theta \leq 35°$ and $0° \leq \phi < 360°$, and their incident power is 1W. For all the users, we consider one LoS path and two non-line-of-sight (NLoS) paths. Normally, the power transmitted along the NLoS path is an order of magnitude less than the power transmitted along the LoS path. Afterwards, channel capacities with the antenna selection scheme introduced in Section IV-A and the lens model analyzed in Section III are simulated and discussed under different scenarios.

Fig. 7 shows the spectrum efficiency against the channel signal-to-noise ratio (SNR) when the system serves different numbers of users simultaneously. In order to avoid the influence introduced from the randomness of the user distribution, the simulation for each number of users working together is repeated for 100 times. It is obvious that the channel capacity is higher at a better SNR for all user numbers. Moreover, when the number of users simultaneously served by the base station increases, the overall system spectrum efficiency also improves. However, more users indicates higher interference power response on the selected antenna for each user. Thence, when the channel SNR is 10 dB, the average channel capacity of each user declines gently from 5.50 bps/Hz for a system with 10 users to 3.01 bps/Hz for that with 60 users due to the stronger interference. A detailed average spectrum efficiency is summarized in Table 1.

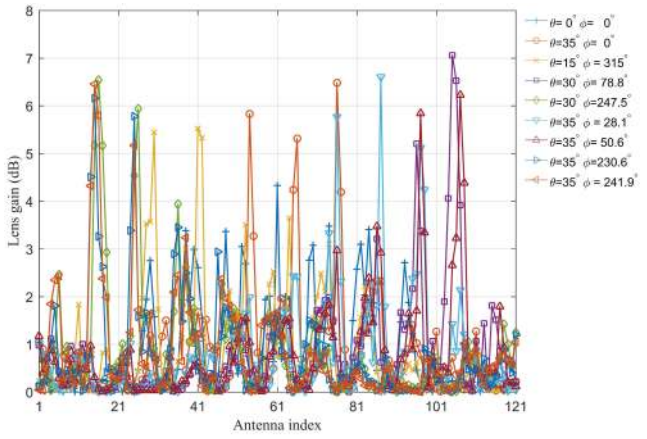

(a)

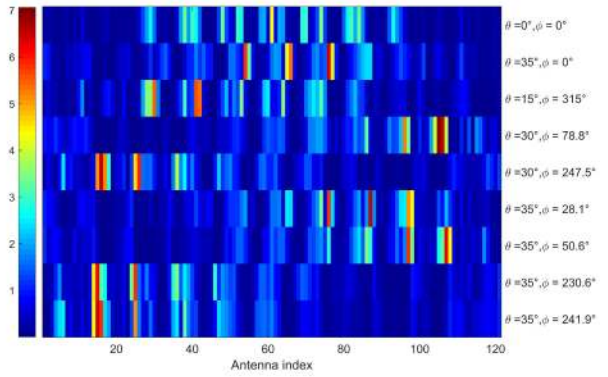

(b)

FIGURE 6. Gains of the metamaterial-based planar lens antenna array for incident waves from different AoAs: (a) 2D gain curves; (b) gain image where the intensity is represented by colored pixels.

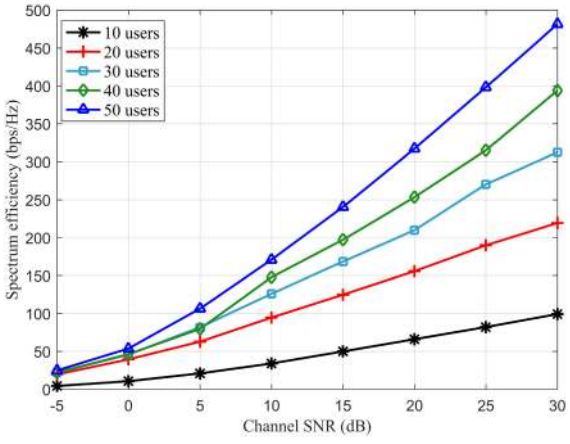

FIGURE 7. Total channel capacity against channel SNR for different user numbers.

V. CONCLUSION

In this paper, we proposed a power profile-based antenna selection strategy for MIMO systems with an all-planar RF-lens antenna array. For practical applications and deployment, the RF-lens antenna consisted of a flat lens made of metamaterials and feeding antenna elements arranged in a 2D plane. By considering the lens and all antenna elements as an entity, the incident field from any user on one antenna body, the electric field radiated by the lens, and the electric field radiated by the rest antenna elements have all been included when characterizing the base station antenna. Then, the received powers of all antennas were derived for incident waves with different angles of arrivals, based on which a decrease maximum capacity antenna selection strategy was achieved. Finally, we analyzed and discussed the MIMO system performance of an all-planar RF lens antenna array operating at 25 GHz with 121 elements.

REFERENCES

[1] THALES. (Dec. 2020). *Introducing 5G Technology and Networks (Speed, Use, Cases and Rollout)*. [Online]. Available: https://www.thalesgroup.com/en/markets/digital-identity-and-security/mobile/inspired/5G

[2] A. Gupta and R. K. Jha, "A survey of 5G network: Architecture and emerging technologies," *IEEE Access*, vol. 3, pp. 1206–1232, Jul. 2015.

[3] I. Parvez, A. Rahmati, I. Guvenc, A. I. Sarwat, and H. Dai, "A survey on low latency towards 5G: RAN, core network and caching solutions," *IEEE Commun. Surveys Tuts.*, vol. 20, no. 4, pp. 3098–3130, 4th Quart., 2018.

[4] M. Agiwal, A. Roy, and N. Saxena, "Next generation 5G wireless networks: A comprehensive survey," *IEEE Commun. Surveys Tuts.*, vol. 18, no. 3, pp. 1617–1655, 3rd Quart., 2016.

[5] W. Yi, Y. Liu, E. Bodanese, A. Nallanathan, and G. K. Karagiannidis, "A unified spatial framework for UAV-aided mmWave networks," *IEEE Trans. Commun.*, vol. 67, no. 12, pp. 8801–8817, Dec. 2019.

[6] I. Messaoudene, H. Youssouf, M. Bilal, M. Belazzoug, and S. Aidel, "Performance improvement of multilayer butler matrix for UWB beamforming antenna," in *Proc. Seminar Detection Syst. Archit. Technol. (DAT)*, Algiers, Algeria, 2017, pp. 1–4.

[7] C. Tsokos, C. Kouloumentas, E. Mylonas, P. Groumas, V. Katopodis, L. Gounaridis, R. B. Timens, R. M. Oldenbeuving, C. G. H. Roeloffzen, and H. Avramopoulos, "Analysis of a multibeam optical beamforming network based on blass matrix architecture," *J. Lightw. Technol.*, vol. 36, no. 16, pp. 3354–3372, Aug. 15, 2018.

[8] D.-C. Kim and S.-O. Park, "Digital beamforming technique with high resolution digital phase shifter and digital phase calibration using SDR," in *Proc. Int. Symp. Antennas Propag. (ISAP)*, Phuket, Thailand, Oct. 2017, pp. 1–2.

[9] Y.-J. Song, S.-J. Lim, S.-K. Lee, and J.-S. Jang, "Adaptive digital beamforming for uplink coverage enhancement in 5G NR system," in *Proc. 27th Telecommun. Forum (TELFOR)*, Belgrade, Serbia, Nov. 2019, pp. 1–4.

[10] X. Yu, J.-C. Shen, J. Zhang, and K. B. Letaief, "Alternating minimization algorithms for hybrid precoding in millimeter wave MIMO systems," *IEEE J. Sel. Topics Signal Process.*, vol. 10, no. 3, pp. 485–500, Apr. 2016.

[11] J. Zhang, X. Huang, V. Dyadyuk, and Y. Guo, "Massive hybrid antenna array for millimeter-wave cellular communications," *IEEE Wireless Commun.*, vol. 22, no. 1, pp. 79–87, Feb. 2015.

[12] J. Cui, Y. Liu, Z. Ding, P. Fan, and A. Nallanathan, "Optimal user scheduling and power allocation for millimeter wave NOMA systems," *IEEE Trans. Wireless Commun.*, vol. 17, no. 3, pp. 1502–1517, Mar. 2018.

[13] J. Zuo, Y. Liu, E. Basar, and O. A. Dobre, "Intelligent reflecting surface enhanced millimeter-wave NOMA systems," *IEEE Commun. Lett.*, vol. 24, no. 11, pp. 2632–2636, Nov. 2020.

[14] F. Rusek, D. Persson, B. Kiong Lau, E. G. Larsson, T. L. Marzetta, and F. Tufvesson, "Scaling up MIMO: Opportunities and challenges with very large arrays," *IEEE Signal Process. Mag.*, vol. 30, no. 1, pp. 40–60, Jan. 2013.

[15] A. Alkhateeb, J. Mo, N. Gonzalez-Prelcic, and R. W. Heath, "MIMO precoding and combining solutions for millimeter-wave systems," *IEEE Commun. Mag.*, vol. 52, no. 12, pp. 122–131, Dec. 2014.

[16] J. Brady, N. Behdad, and A. M. Sayeed, "Beamspace MIMO for millimeter-wave communications: System architecture, modeling, analysis, and measurements," *IEEE Trans. Antennas Propag.*, vol. 61, no. 7, pp. 3814–3827, Jul. 2013.

[17] X. Gao, L. Dai, Z. Chen, Z. Wang, and Z. Zhang, "Near-optimal beam selection for beamspace mmWave massive MIMO systems," *IEEE Commun. Lett.*, vol. 20, no. 5, pp. 1054–1057, May 2016.
[18] Y. Zeng, R. Zhang, and Z. N. Chen, "Electromagnetic lens-focusing antenna enabled massive MIMO: Performance improvement and cost reduction," *IEEE J. Sel. Areas Commun.*, vol. 32, no. 6, pp. 1194–1206, Jun. 2014.
[19] R. Qian, M. Sellathurai, and X. M. Fang, "Antenna selection for multi-user MIMO at millimeter-wave spectrum with lens antenna arrays," in *Proc. IEEE Int. Conf. Commun. (ICC)*, Paris, France, May 2017, pp. 1–5.
[20] Y. Gao, M. Khaliel, F. Zheng, and T. Kaiser, "Rotman lens based hybrid analog–digital beamforming in massive MIMO systems: Array architectures, beam selection algorithms and experiments," *IEEE Trans. Veh. Technol.*, vol. 66, no. 10, pp. 9134–9148, Oct. 2017.
[21] X. Gao, L. Dai, S. Han, C.-L. I, and X. Wang, "Reliable beamspace channel estimation for millimeter-wave massive MIMO systems with lens antenna array," *IEEE Trans. Wireless Commun.*, vol. 16, no. 9, pp. 6010–6021, Sep. 2017.
[22] L. Yang, Y. Zeng, and R. Zhang, "Channel estimation for millimeter-wave MIMO communications with lens antenna arrays," *IEEE Trans. Veh. Technol.*, vol. 67, no. 4, pp. 3239–3251, Apr. 2018.
[23] J. Ala-Laurinaho, J. Aurinsalo, A. Karttunen, M. Kaunisto, A. Lamminen, J. Nurmiharju, A. V. Raisanen, J. Saily, and P. Wainio, "2-D beam-steerable integrated lens antenna system for 5G *E*-band access and backhaul," *IEEE Trans. Microw. Theory Techn.*, vol. 64, no. 7, pp. 2244–2255, Jul. 2016.
[24] B. Wang, L. Dai, Z. Wang, N. Ge, and S. Zhou, "Spectrum and energy-efficient beamspace MIMO-NOMA for millimeter-wave communications using lens antenna array," *IEEE J. Sel. Areas Commun.*, vol. 35, no. 10, pp. 2370–2382, Oct. 2017.
[25] M. A. Almasi, R. Amiri, M. Vaezi, and H. Mehrpouyan, "Lens-based millimeter wave reconfigurable antenna NOMA," in *Proc. IEEE Int. Conf. Commun. Workshops (ICC Workshops)*, Shanghai, China, May 2019, pp. 1–5.
[26] Y. Zeng and R. Zhang, "Millimeter wave MIMO with lens antenna array: A new path division multiplexing paradigm," *IEEE Trans. Commun.*, vol. 64, no. 4, pp. 1557–1571, Apr. 2016.
[27] Y. Zeng, L. Yang, and R. Zhang, "Multi-user millimeter wave MIMO with full-dimensional lens antenna array," *IEEE Trans. Wireless Commun.*, vol. 17, no. 4, pp. 2800–2814, Apr. 2018.
[28] A. Sayeed and N. Behdad, "Continuous aperture phased MIMO: Basic theory and applications," in *Proc. 48th Annu. Allerton Conf. Commun., Control, Comput. (Allerton)*, Spokane, WA, USA, Sep. 2010, pp. 1196–1203.
[29] P. Lau, Z. N. Chen, and X. Qing, "Electromagnetic field distribution of lens antennas," in *Proc. Asia–Pacific Conf. Antennas Propag.*, Aug. 2013, pp. 1–2.
[30] T. Kwon, Y.-G. Lim, B.-W. Min, and C.-B. Chae, "RF lens-embedded massive MIMO systems: Fabrication issues and codebook design," *IEEE Trans. Microw. Theory Techn.*, vol. 64, no. 7, pp. 2256–2271, Jul. 2016.
[31] R. Sauleau and B. Bares, "A complete procedure for the design and optimization of arbitrarily shaped integrated lens antennas," *IEEE Trans. Antennas Propag.*, vol. 54, no. 4, pp. 1122–1133, Apr. 2006.
[32] B. Chantraine-Bares, R. Sauleau, L. Le Coq, and K. Mahdjoubi, "A new accurate design method for millimeter-wave homogeneous dielectric substrate lens antennas of arbitrary shape," *IEEE Trans. Antennas Propag.*, vol. 53, no. 3, pp. 1069–1082, Mar. 2005.
[33] M. Jiang, Z. N. Chen, Y. Zhang, W. Hong, and X. Xuan, "Metamaterial-based thin planar lens antenna for spatial beamforming and multi-beam massive MIMO," *IEEE Trans. Antennas Propag.*, vol. 65, no. 2, pp. 464–472, Feb. 2017.
[34] B. Orazbayev, M. Beruete, V. Pacheco-Peña, G. Crespo, J. Teniente, and M. Navarro-Cía, "Soret fishnet metalens antenna," *Sci. Rep.*, vol. 5, no. 1, pp. 1–7, May 2015.
[35] S. A. Kuznetsov, M. A. Astafev, M. Beruete, and M. Navarro-Cía, "Planar holographic metasurfaces for terahertz focusing," *Sci. Rep.*, vol. 5, no. 1, pp. 1–8, Jan. 2015.
[36] A. Forenza, D. J. Love, and R. W. Heath, Jr., "Simplified spatial correlation models for clustered MIMO channels with different array configurations," *IEEE Trans. Veh. Technol.*, vol. 56, no. 4, pp. 1924–1934, Jul. 2007.
[37] B. Ottersten, "Array processing for wireless communications," in *Proc. 8th IEEE Signal Process. Workshop Stat. Signal Array Process.*, Davos, Switzerland, Jun. 1996, pp. 466–473.
[38] M. Rutschlin, T. Wittig, and Z. Iluz, "Phased antenna array design with CST studio suite," in *Proc. 10th Eur. Conf. Antennas Propag. (EuCAP)*, Davos, Switzerland, Apr. 2016, pp. 1–5.
[39] X.-M. Sun, M.-L. Yang, and X.-Q. Sheng, "Accurate and efficient analysis of large antenna arrays with radome on a large aircraft," *Prog. Electromagn. Res.*, vol. 153, pp. 103–111, 2015.
[40] P. V. Amadori and C. Masouros, "Low RF-complexity millimeter-wave beamspace-MIMO systems by beam selection," *IEEE Trans. Commun.*, vol. 63, no. 6, pp. 2212–2223, Jun. 2015.

QIANYUN ZHANG (Member, IEEE) received the B.Sc. degree from the Beijing University of Posts and Telecommunications, Beijing, China, in 2014, and the Ph.D. degree from the Queen Mary University of London, London, U.K., in 2018. She has been a Lecturer (an Assistant Professor) with the School of Cyber Science and Technology, Beihang University, since 2018. She is currently an Editor on the Editorial Board of the IEEE Open Journal of Antennas and Propagation. Her research interests include antennas and propagation theory, novel antenna arrays, and the Internet of Things securities.

XINWEI LI (Student Member, IEEE) received the B.E. degree from Beihang University, Beijing, China, in 2020, where he is currently pursuing the M.Sc. degree with the School of Cyber Science and Technology. His current research interests include wireless network security and signal feature extraction and analysis.

LEI CHENG received the B.Eng. degree from Zhejiang University, in 2013, and the Ph.D. degree from the University of Hong Kong, in 2018. He is currently a Research Scientist with the Shenzhen Research Institute of Big Data. His research interests include tensor data analytics, statistical inference, and large-scale optimization.

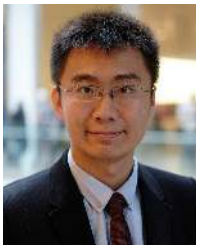

YUANWEI LIU (Senior Member, IEEE) received the B.S. and M.S. degrees from the Beijing University of Posts and Telecommunications, in 2011 and 2014, respectively, and the Ph.D. degree in electrical engineering from the Queen Mary University of London, U.K., in 2016.

He was with the Department of Informatics, King's College London, from 2016 to 2017, where he was a Postdoctoral Research Fellow. He has been a Lecturer (an Assistant Professor) with the School of Electronic Engineering and Computer Science, Queen Mary University of London, since 2017. His research interests include 5G/6G networks, the Internet of Things, machine learning, and stochastic geometry. He is currently an Editor on the Editorial Board of the IEEE TRANSACTIONS ON COMMUNICATIONS, and IEEE COMMUNICATIONS LETTERS. He also serves as a Guest Editor for IEEE JSTSP special issue on Signal Processing Advances for Non-Orthogonal Multiple Access in Next Generation Wireless Networks. He has served as a TPC Member for many IEEE conferences, such as GLOBECOM and ICC. He received the Exemplary Reviewer Certificate of IEEE WIRELESS COMMUNICATIONS LETTERS, in 2015, IEEE TRANSACTIONS ON COMMUNICATIONS, in 2016 and 2017, and IEEE TRANSACTIONS ON WIRELESS COMMUNICATIONS, in 2017 and 2018. He has served as the Publicity Co-Chair for VTC 2019-Fall. He is the leading contributor for Best Readings for Non-Orthogonal Multiple Access (NOMA) and the primary contributor for Best Readings for Reconfigurable Intelligent Surfaces (RIS). He serves as Tutorials and Invited Presentations Officer for Reconfigurable Intelligent Surfaces Emerging Technology Initiative, the Vice-Chair Special Interest Group (SIG) Wireless Communications Technical Committee (WTC) on the topic of Reconfigurable Intelligent Surfaces for Smart Radio Environments (RISE).

YUE GAO (Senior Member, IEEE) received the Ph.D. degree from the Queen Mary University of London (QMUL), U.K., in 2007.

He was a Lecturer, a Senior Lecturer, and a Reader in antennas and signal processing with QMUL. He is currently a Professor of wireless communications with the Institute for Communication Systems, University of Surrey, U.K. He also leads a team developing fundamental research into practice in the interdisciplinary area of smart antennas, signal processing, spectrum sharing, millimetre-wave, and the Internet of Things technologies in mobile and satellite systems. He has published more than 180 peer-reviewed journal and conference papers, three patents, one book and five book chapters, and three best paper awards. He is also an Engineering and Physical Sciences Research Council Fellow since 2018 to 2023. He was a co-recipient of the EU Horizon Prize Award on Collaborative Spectrum Sharing in 2016, and shortlisted for the Newton Prize on IoT systems for smart farming in 2019. He served as the Signal Processing for Communications Symposium Co-Chair for IEEE ICCC 2016, the Publicity Co-Chair for the IEEE GLOBECOM 2016, the Cognitive Radio Symposium Co-Chair for the IEEE GLOBECOM 2017, and the General Chair of the IEEE WoWMoM and iWEM 2017. He is the Chair of the IEEE Technical Committee on Cognitive Networks, the Secretary of the IEEE ComSoc Technical Committee Wireless Communication and the IEEE Distinguished Lecturer of the Vehicular Technology Society. He is an Editor of the IEEE INTERNET OF THINGS JOURNAL, IEEE TRANSACTIONS ON VEHICULAR TECHNOLOGY, and IEEE TRANSACTIONS ON COGNITIVE NETWORKS.